Journal of Heat and Mass Transfer Research 9 (2022) 77- 84

Semnan University

Journal of Heat and Mass Transfer Research

Journal homepage: https://jhmtr.semnan.ac.ir

Converging Flow Passages, Nanofluids and Magnetic Field: Effects on the Thermal Response of Microchannel Heat Sinks

Amir Fattahi[a], Maziar Dehghan[*,b], Mohammad Sadegh Valipour[a]

[a] Faculty of Mechanical Engineering, Semnan University, Semnan, Iran.
[b] Department of Energy, Material and Energy Research Center (MERC), Tehran, Iran.

PAPER INFO

Paper history:
Received: 2020-12-04
Revised: 2022-07-04
Accepted: 2022-07-16

Keywords:
Nanofluid;
Converging flow passage;
Convective heat transfer;
Microchannel;
Magnetic field.

ABSTRACT

To analyze the possibility of heat transfer enhancement of micro-scale heat exchangers, the transport phenomena of water (H_2O) - Aluminum oxide (Al_2O_3) nanofluid in a three-dimensional microchannel with converging flow passages in the presence of a magnetic field are numerically investigated. All simulations are performed for the Harman number (Ha) of 0-20 and the volume fraction of $\emptyset$ = 0 and 0.02 in the laminar regime (Reynolds number, Re, < 100). The magnetic field is applied in the normal direction (with respect to the flow direction). The results show that the convection heat transfer coefficient, as well as the friction factor, increases with the increase of the Hartman number. The increase in the friction factor is noticeable up to being doubled while the increase of the convection heat transfer coefficient is up to 20 %. The uniform velocity arising from the magnetic field presence gives almost uniform temperature distributions in the fluid and solid parts of the micro-channel, which makes removing higher heat fluxes within the safe temperature limit possible. Although the heat transfer performance enhances with the increase of the magnetic field, the rate of heat transfer enhancement decreases with the increasing magnetic field. In other words, the magnetic field has a maximum effective value and there is no justification for a further increase according to the energy efficiency perspectives. It should be noted that the mentioned limits for magnetic field (here, presented with Ha) are very high and almost impossible to be applied at micro-scales. In addition, the effect of the magnetic field on the velocity profile decreases with the increase of the passage convergence. In other words, the flow convergence eliminates the need for a high magnetic field to have a uniform velocity profile and as well a uniform temperature distribution.

DOI: 10.22075/jhmtr.2022.22016.1320

1. Introduction

The technological advances of the electronics industry and the need to create small-sized devices result in the issue of removing high heat generated per unit area or volume. One of the most practical solutions to the above-mentioned problem is the microchannel heat sinks (MCHS) because of several advantages like small dimensions, high surface area to volume ratio, high thermal conductivity in the solid part, and small volume of coolant fluid requirement [1, 2].

Osanloo et al. [3] considered a double layer MCHS with tapered lower and upper channels. They showed that the temperature of the bottom of MCHS decreases by increasing the convergence angle of channels. Bijan et al. [4] showed that the optimal distance between the plates in the microchannels is proportional to $({}^{\mu\alpha}/_{\Delta p l^2})^2$ wherein μ is the viscosity of the fluid, α is the thermal diffusion coefficient and Δp is the pressure drop. Li et al. [5] investigated the forced convection heat transfer in microchannels with different aspect ratios showing that variation of the thermophysical properties may give considerable changes in the results. Gamrat et al. [6] analyzed the convective heat transfer in microchannels. Contrary to the experimental work, the thermal entrance phenomenon did not affect the heat transfer rate significantly for spacing less than 1 millimeter in their numerical analysis.

*Corresponding Author: Maziar Dehghan
Email: dehghan.maziar@gmail.com, ma.dehghan@merc.ac.ir

Within the past decades, it has been confirmed that adding nanoparticles to base liquids can increase the heat transfer abilities [7, 8] and it can be considered a passive [9] as well as an active enhancement technique. Koo and Kleinstreuer [10] showed that adding nanoparticles with an average diameter of 20 nm and volume fraction of $1 < \emptyset < 4\%$ to high-Prandtl fluids significantly increases the heat transfer ability of the fluid. Jang et al. [11] investigated the cooling performance of diamond nanofluid flow in micro-channels under a defined pumping power of 2.5 W and showed that the micro-channel thermal performance of a fluid containing diamond particles increased about 10% compared to the pure base fluid. Gao et al. [12] investigated the heat transfer and flow of copper oxide nanofluids in rectangular microchannels for different volume fractions. They reported an increase in the heat transfer rate with a relatively low increase in the pressure drop. Fornalik-Wajs et al. [13] found that using nanoparticles and a magnetic field shows a synergistic effect with higher efficiency. Hung et al. [14] by optimizing various channel configurations showed that the distribution of thermal flux in width-tapered channels compared to other geometries such as single-layered- (SL) or double-layered- (DL) MCHS are more uniform. He et al. [15] investigated the effects of the various nanoparticle sizes, concentrations and Reynolds number on the flow and the convective heat transfer behavior. They found that the mentioned parameters are important, especially in the entrance region. Mirzaei and Dehghan [16] revealed that the assumption of the temperature-dependent thermophysical properties is more accurate than the assumption of constant properties for the case of nanofluid flows in microchannel heat sinks. Chein et al. [17] studied Cu-water nanofluid flow in a microchannel heat sink as the coolant with superior thermal performance. Peng et al. [18] revealed that applying nanofluids in solar collectors is accompanied by higher total efficiency. Wang et al. [19] found that nanofluids could be useful in increasing the thermochemical performance of a solar receiver. Liang et al. [20] developed an improved calculation model for the spectral radiation characteristics of nanofluids to increase the efficiency of capturing specific spectrum photons by adjusting the spatial distribution of particles. After optimization of nanoparticle size distribution and volume fraction, Liang et al. [21] verified the feasibility of using a cost-effective glycol-ZnO nanofluid in spectral splitting CPV/T system by outdoor experiments.

Aminfar et al. [22] investigated flows in a vertical tube under a non-uniform magnetic field. They showed that a magnetic field with a negative gradient increases the Nusselt number and the required pumping power. Wrobel et al. [23] worked on a new governing equation of heat transfer under a magnetic field. The effects of some different types of magnetic fields in two-dimensional flow on the resistance coefficient have been experimentally investigated by Sawada et al. [24]. Their experiments revealed that there would be a relation between the strength of the magnetic field and the length scale. Selimli et al. [25] numerically studied magnetic effects on the liquid lithium flow in a rectangular duct. They found that by applying a magnetic field the hydrodynamic properties of electrically conductive fluids can be controlled. Zhao and Hu [26] experimentally found that by variation of the magnetic field, the density of the fluid can be changed. Hajialigol et al. [27] numerically investigated nanofluid flow in a three-dimensional microchannel in the presence of a magnetic field and reported an increase in the heat transfer rate by increasing the intensity of the magnetic field. Aminfar et al. [28] revealed that the magnetic field increases the Nusselt number and the coefficient of friction. Ganguly et al. [29] showed that the vortices created along the wall under the influence of the magnetic field cause a change in the temperature distribution and increase the heat transfer coefficient. Fadaei et al. [30] studied the nanofluid flow and heat transfer in a three-dimensional tube in the presence of a magnetic field. They showed by applying the magnetic field of 3×10^5 (A/m) the Nusselt number value can be increased by 196%.

Zeng et al. [31] analyzed the particle separation for the case of two permanent magnets used for ferrofluid flow in a minichannel. Sheikholeslami et al. [32] examined CuO–water nanofluid flow in an enclosure under a constant heat flux imposed from the bottom in the presence of a magnetic field. They showed as the Hartmann number increases, the heat transfer coefficient increases. The use of transverse magnetic force for particle separation is observed in a series of papers [33, 34].

To boost the cooling effects, the idea of nanofluid-cooled microchannel heat sinks (MCHS) enhanced by width-tapered walls has been recently verified by Dehghan et al. [35, 36]. In the present study, a magnetic field is applied to investigate the possibility of further uniformization of the cross-sectional temperature distribution. Using the finite volume method (FVM), heat and fluid flow for different conditions are investigated for Hartman numbers ranging between 0 and 20. Despite many discussions, in the case of tapered microchannels [37], there are still unresolved issues in this regard while no magnetic effects have been considered up to now. Both hydrodynamic and thermal characteristics in terms of friction factor (C_{fx}), the dimensionless velocity profile (U), and heat transfer coefficient (h_z) as well as contours of velocity and temperature fields are analyzed and discussed.

2. Mathematical modeling

The schematic diagram considered in this study is seen in Fig. 1. Table 1 presents the dimensions of the schematic geometry. γ is the ratio of the channel entrance width to the channel outlet width and D_h is the hydraulic diameter. The length L_1 (shown in Fig. 1) is under the influence of a constant magnetic field (B_0). A constant heat flux (q'') equal to 100 W/cm^2 is imposed on the bottom surface of the MCHS. Al_2O_3 particles are used with the mean diameter of 38.4 nm (Table 2). The inlet temperature of the water–Al_2O_3 nanofluid is 293 K.

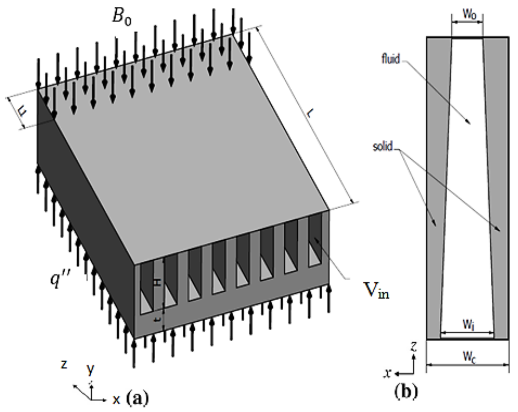

Figure 1. (a) Schematic diagram and (b) top view of a single channel [37]

Table 1. Microchannel dimensions [37]

Wi (μm)	Wo (μm)	Wc (μm)	H (μm)	L (μm)	L1 (μm)	t (μm)
200	200, 150, 100, 75	400	1000	12000	3000	500

Table 2. Nano-particle (Al_2O_3) properties [16]

ρ_p (kg/m^3)	3,970
C_p (w/kgK)	760
K_p(W/mK)	40

2.1. Governing equations

Governing equations for the fluid part are:

$$\frac{\partial U}{\partial X}+\frac{\partial V}{\partial Y}+\frac{\partial W}{\partial Z}=0 \tag{1}$$

$$U\frac{\partial U}{\partial X}+V\frac{\partial U}{\partial Y}+W\frac{\partial U}{\partial Z}=-\frac{\partial P}{\partial X}+\frac{\mu_{nf}}{\rho_{nf}\alpha_f}\frac{1}{Re\,Pr}\left(\frac{\partial^2 U}{\partial X^2}+\frac{\partial^2 U}{\partial Y^2}+\frac{\partial^2 U}{\partial Z^2}\right)-\frac{Ha^2}{Re}U \tag{2}$$

$$U\frac{\partial V}{\partial X}+V\frac{\partial V}{\partial Y}+W\frac{\partial V}{\partial Z}=-\frac{\partial P}{\partial Y}+\frac{\mu_{nf}}{\rho_{nf}\alpha_f}\frac{1}{Re\,Pr}\times\left(\frac{\partial^2 V}{\partial X^2}+\frac{\partial^2 V}{\partial Y^2}+\frac{\partial^2 V}{\partial Z^2}\right) \tag{3}$$

$$U\frac{\partial W}{\partial X}+V\frac{\partial W}{\partial Y}+W\frac{\partial W}{\partial Z}=-\frac{\partial P}{\partial Z}+\frac{\mu_{nf}}{\rho_{nf}\alpha_f}\frac{1}{Re\,Pr}\times\left(\frac{\partial^2 W}{\partial X^2}+\frac{\partial^2 W}{\partial Y^2}+\frac{\partial^2 W}{\partial Z^2}\right)-\frac{Ha^2}{Re}W \tag{4}$$

$$U\frac{\partial \theta}{\partial X}+V\frac{\partial \theta}{\partial Y}+W\frac{\partial \theta}{\partial Z}=-\frac{\partial P}{\partial Z}+\frac{\alpha_{nf}}{\alpha_f}\frac{1}{Re\,Pr}\left(\frac{\partial^2 \theta}{\partial X^2}+\frac{\partial^2 \theta}{\partial Y^2}+\frac{\partial^2 \theta}{\partial Z^2}\right) \tag{5}$$

the energy conservation equation for the solid part is:

$$k_s\left(\frac{\partial^2 \theta}{\partial X^2}+\frac{\partial^2 \theta}{\partial Y^2}+\frac{\partial^2 \theta}{\partial Z^2}\right)=0 \tag{6}$$

2.2. Boundary conditions

Because of the symmetry (Fig. 2), half of MCHS is considered for the numerical study. The boundary conditions are mathematically presented in table 3.

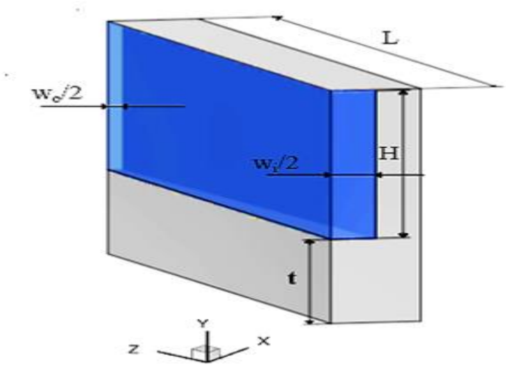

Figure 2. Schematic of the considered computational cell of the microchannel

Table 3. Boundary conditions considered in this research

Boundary	Condition
$x = {}^{W_c}/_2$, $0 < y < t$, $0 < z < L$	$\frac{\partial T}{\partial X}=0$
$x=\frac{W_c-W_i}{2}$, $t < y < H+t$, $0 < Z < L$	$k_s\frac{\partial T}{\partial x}\Big\vert_s = k_f\frac{\partial T}{\partial x}\Big\vert_f$, $T_s = T_f$, $u=v=w=0$
$x = 0$, $t < y < H+t$, $0 < Z < L$	$\frac{\partial T}{\partial X}=0$
$x = {}^{W_c}/_2$, $t < y < t+H$, $0 < z < L$	$\frac{\partial T}{\partial x}=0$, $\frac{\partial u}{\partial x}=0$
$z = L$, $\frac{W_c-W_o}{2}\le x\le\frac{W_c}{2}$, $t < y < H+t$	$p = p_{out}$
$z = 0$, $\frac{W_c-W_i}{2}\le x\le\frac{W_c}{2}$, $t < y < H+t$	$w = V_{in}$or, $u=v=0$
$y = t+H$, $o < x\le\frac{W_c}{2}$, $0 < Z < L$	$\frac{\partial T}{\partial y}=0$,$u=v=w=0$
$y=t$, $\frac{W_c-W_i}{2}\le x\le\frac{W_c}{2}$, $0 < Z < L$	$k_s\frac{\partial T}{\partial y}\Big\vert_s = k_f\frac{\partial T}{\partial y}\Big\vert_f$, $T_s = T_f$, $u=v=w=0$
$y=0$, $o < x\le\frac{W_c}{2}$, $0 < Z < L$	$q'' = 100\,\frac{W}{Cm^2}$
$y=t+H, 0\le x\le\frac{W_c-W_o}{2}$, $0 < Z < L$	$\frac{\partial T}{\partial y}=0$

2.3. Numerical method

The numerical analysis is based on the development of the study by Hung et al. [14] and Dehghan et al. [37] adopting a simple algorithm (SIMPLE) to solve the non-linear fluid flow and heat transfer conservation equations using the finite volume method [37]. The second-order upwind method is used or discretization. The selected mesh (x×y×z=20×50×100) shows only a 3% maximum difference with a finer one (x×y×z=30×75×150) in comparing dimensionless bulk mean temperature along the channel.

2.4. Fluid properties

The thermophysical parameters of the nanofluid are:

$$\rho_{nf} = (1-\emptyset)\rho_{bf} + \emptyset\rho_p \tag{7}$$

$$(\rho C_p)_{nf} = (1-\emptyset)(\rho C_p)_{bf} + \emptyset(\rho C_p)_p \tag{8}$$

$$\sigma_{nf} = (1-\emptyset)\sigma_{bf} + \emptyset\sigma_p \tag{9}$$

According to Koo and Kleinstreuer [8], effective thermal conductivity and effective viscosity are composed of two parts, the nanoparticle's conventional static part, and a Brownian motion part:

$$k_{eff} = k_{static} + k_{Brownian} \tag{10}$$

$$\frac{k_{static}}{k_{bf}} = 1 + \frac{3(\frac{k_p}{k_{bf}}-1)\emptyset}{\left(\frac{k_p}{k_{bf}}+2\right) - (\frac{k_p}{k_{bf}}-1)\emptyset} \tag{11}$$

$$k_{Brownian} = 5\times10^4\beta\emptyset\rho C_P\sqrt{\frac{KT}{\rho_{Pd_p}}}\,f(T.\emptyset) \tag{12}$$

the functions β and f were introduced in [31].

$$\mu_{eff} = \mu_{static} + \mu_{Brownian} \tag{13}$$

$$\mu_{Brownian} = \frac{k_{Brownian}}{k_{bf}} \times \frac{\mu_{bf}}{pr_{bf}} \tag{14}$$

To obtain the results in the general form, first dimensionless parameters should be defined. The surface friction coefficient is defined by equation (15):

$$C_{f,z} = \frac{\tau_{wall}(z)}{\frac{1}{2}\rho u^2{}_{ave}} \tag{15}$$

u_{ave} is the average cross-sectional velocity and $\tau_{wall}(z)$ is the shear stress. The convection heat transfer coefficient is defined as follows:

$$h_z = \frac{q_w(z)}{T_w(z) - T_b(z)} \tag{16}$$

$T_b(z)$ and $T_w(z)$ represent the bulk-mean and wall temperature of the fluid. $T_b(z)$ is defined as follows:

$$T_b(z) = \frac{\int_{A_c}\rho u c_p T_f dA}{\int_{A_c}\rho u c_p\, dA} \tag{17}$$

In equation (16) $q_w(z)$ is the heat flux imposed from the wall to the fluid and is calculated by Eq. (18):

$$q_w(z) = \frac{\sum_\Gamma q(x,y,z)\,\mathrm{dA}(x,y,z)}{\sum_\Gamma \mathrm{dA}(x,y,z)} \tag{18}$$

Γ represents the perimeter of the channel.

3. Results and Discussion

Fig. 3 shows the dimensionless velocity profile ($U = u\ /\ u_{ave}$) on the mid-plane of the channel in the y-direction (H/2) and at $Z = 33$ for different convergence rations (γ). From the momentum equation, it can be seen that the magnetic force on the fluid of flow is proportional to the velocity and in the opposite direction. On the other hand, the maximum velocity occurs at the center of the channel. Therefore, the magnetic force shows the maximum opposite force at the channel center. So, the velocity increases near the channel wall in order to satisfy the continuity equation, and hence the velocity profile becomes almost flat. It can also be seen that an increase in the convergence reduces the impact of the magnetic field on the flow due to flatting the velocity because of the channel convergence [35, 37].

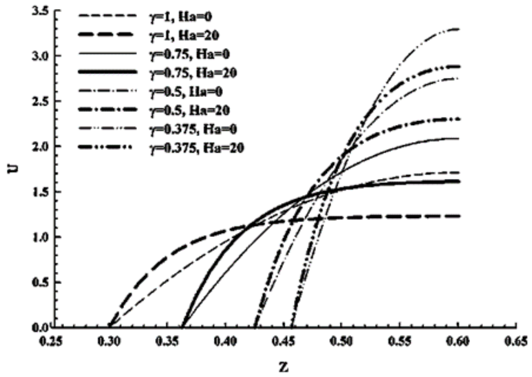

Figure 3. Centerline dimensionless velocity profile at position Z=33.3 for different channel convergence ratios

Fig. 4 shows the contours of the centerline dimensionless velocity for the constant Ha number of 20 and for different convergence ratio (γ) values of 0.375 and 1. It is seen that the velocity of the fluid reaches its maximum value at the centerline. A comparison between Fig. 4(a) and Fig. 4(b) reveals that the convergence of the walls causes the fluid to accelerate and hence the centerline velocity of the channel with converging walls (γ = 0.375) in Fig. 4(b) shows higher values (almost twice) than the straight channel (γ = 1).

Moreover, it can be seen in Fig. 4 that the velocity field becomes almost uniform for both channels with parallel and converging walls from the point where the magnetic field is inserted to the bottom of the channels.

As it was seen in Fig 3, the velocity distribution in the converging channel (γ = 0.375) is more uniform compared to the straight channel (γ = 1), which is the result of a higher axial velocity and a stronger Lorentz force as well.

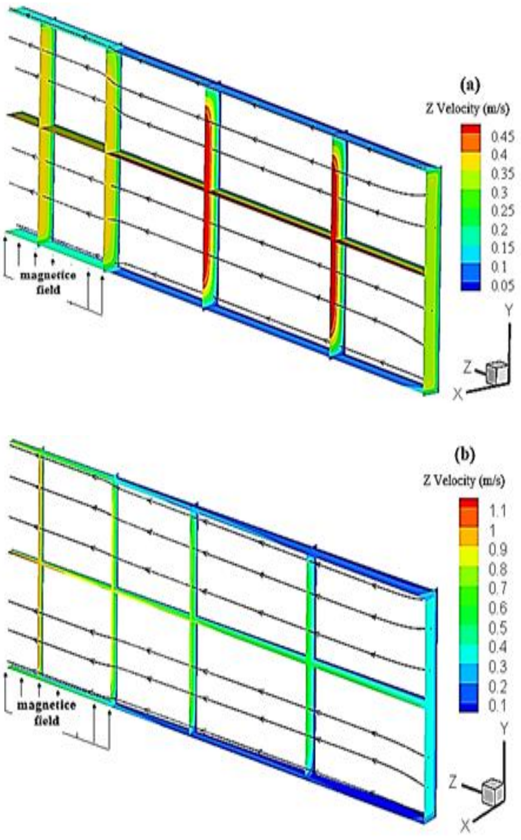

Figure 4. Velocity contours for Ha=20
(a) $\gamma = 1$ and (b) $\gamma = 0.375$

Fig. 5 shows the friction factor (Cf,z) in a channel with a varying aspect ratio (i.e. a channel with converging walls) for Hartmann numbers of 0 and 20. In the entrance region, C_(f"," z) changes from a very large value and reaches an almost constant value along the channel because of the development of the hydrodynamic boundary layer. According to Eq. (15), the friction coefficient is proportional to ∂u/∂n, wherein n is the normal direction. Along the flow direction and with the development of the hydrodynamic boundary layer, the velocity gradient (∂u/∂n) decreases. So that, the coefficient of friction decreases. By inserting the magnetic field, the velocity becomes more uniform along the cross-sectional area. It means that the velocity should increase in near-wall regions. Hence, the velocity gradient (∂u/∂n) and consequently the friction factor increases. For a converging channel, since the average velocity increases along the flow direction, the dynamic pressure (ρu_ave^2) seen in Eq. (15) increases which leads to a reduction in the friction factor.

The heat transfer coefficient (Eq. 16) for different convergences and Hartmann numbers is depicted in Fig. 6. In the entrance region, wherein the thermal boundary layer thickness is thin, the convection heat transfer coefficient shows the maximum value. With the increase of the thermal boundary layer, the thermal resistance increase and hence the convection heat transfer coefficient decreases.

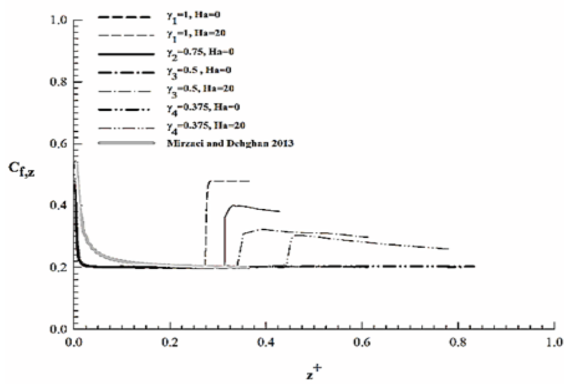

Figure 5. Friction factor ($C_{f,z}$) Ha = 0 and 20

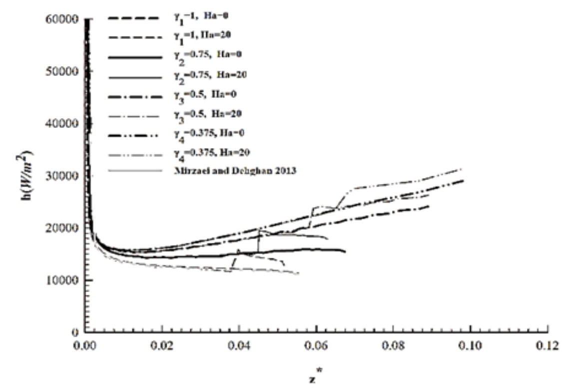

Figure 6. Effects of the magnetic field and channel convergence on the convection heat transfer coefficient

In a converging channel, because of the increase in the velocity magnitude, the heat transfer coefficient tends to increase along the channel. The reduction caused by the boundary layer thickness growth is balanced by this tendency originated by the velocity magnitude increment. So, the convection heat transfer coefficient starts to increase from somewhere just after the entrance region.

As obtained previously, the velocity field becomes almost uniform by applying the magnetic field. Such an almost uniform velocity translates to a very thin hydrodynamic boundary layer which yields a step-wise increase in the convection heat transfer coefficient as seen for cases with Ha = 20. The maximum heat transfer coefficient belongs to the most converging channel (γ = 0.375) with the highest magnetic field (Ha = 20).

One of the most important issues concerning the microchannel heat sinks is the highest temperature occurring on the bottom side where the heat flux is applied and the hot spots may occur. To find out the effects of the channel convergence and the applied magnetic field on the maximum temperature, Fig. 7 is plotted. It shows the temperature of the bottom side of the microchannel heat sink where the heat flux is imposed. According to the discussion presented previously, the lowest temperature corresponds to the case of the most converging channel ($\gamma = 0.375$) and the strongest applied magnetic field (Ha = 20). It is worth noting that the influence of channel convergence is more apparent than the applied magnetic field. In other words, there almost would not be any need to apply a magnetic field and consume more energy to enhance the heat transfer rate and to decrease the hot spot temperatures if the converging channels are used. It is worth mentioning that such high magnetic fields required to reach such high Ha numbers as high as 20 are almost impossible at microscales in the application. So that the mentioned points confirm the applicability and the effectiveness of using the converging flow passages idea. To have a more general look at the thermal field, Fig. 8 is presented which shows the temperature in a 3D view. According to what has been discussed, a reduction in the temperature of the solid part of the microchannel from cases a to d (obtained from magnetic field and channel convergence) is seen.

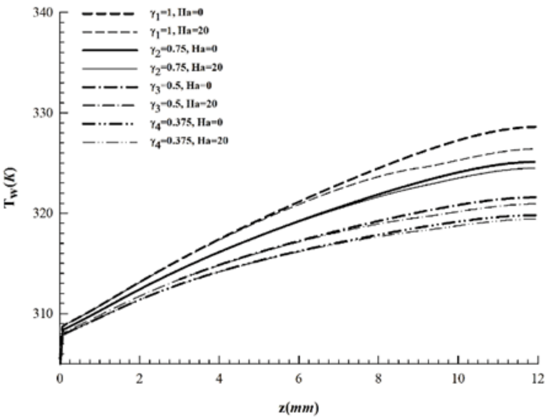

Figure 7. The temperature of the bottom surface of MCHS

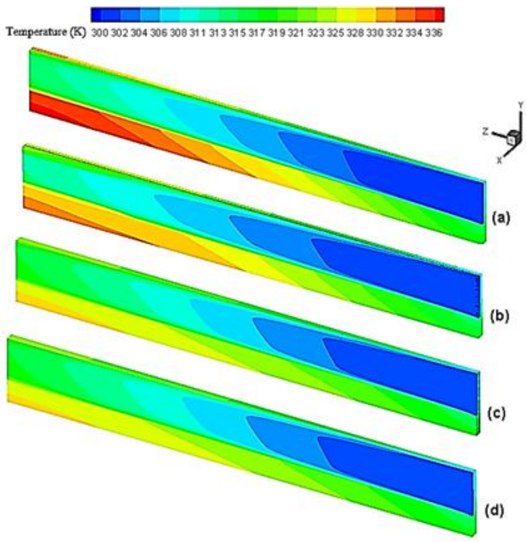

Figure 8. Temperature contours for: (a) Ha=0 and γ=1; (b) Ha=20 and γ=1; (c) Ha=0 and γ=0.375; (d) Ha=20 and γ=0.375

Conclusion

In this paper, transport phenomena of water (H2O)-Aluminum oxide (Al2O3) in a three-dimensional microchannel with different convergence ratios under a magnetic field were numerically investigated. The results showed that the magnetic field makes the velocity distribution more uniform, and hence the friction factor increases up to two times. In contrast, the friction coefficient decreases because by converging the flow passages because of an increment in the average velocity and the dynamic pressure as well. Moreover, a transverse magnetic field augmented the convection heat transfer coefficient as well as using converging channels. But, the influence of the magnetic field on the heat transfer rate enhancement and on reducing the bottom-side wall temperature of MCHSs diminishes by increasing the convergence of the flow passages. In other words, using converging flow passages shows the strongest effects and the best heat transfer augmentation among other heat transfer rate enhancement techniques considered in the present study. Using converging flow passages gives almost the best heat transfer performance with no need to use any other energy-consuming heat transfer enhancement technique.

Nomenclature

B	Magnetic field intensity (T)
D_h	Hydraulic diameter (2WH/(W+H)) (m)
H	Height (m)
Ha	Hartman number (B $D_h\sqrt{\frac{\sigma_{nf}}{\rho_{nf}\nu_{bf}}}$)
P	Pressure (Pa)
Pr	Prandtl number ($\frac{\nu_{bf}}{\alpha_{bf}}$)
Q"	Heat flux (W/m^2)
Re	Reynolds number ($\frac{u_{in}D_{h_{in}}}{\nu_{bf}}$)
t	Thickness (m)
T	Temperature (K)
u, v, w	Components of velocity
U, V, W	Dimensionless velocity components (u/u_{in}, v/u_{in}, w/u_{in})
x, y, z	Cartesian coordinates (m)
X, Y, Z	Dimensionless Cartesian coordinates ($x/D_{h_{in}}$, $y/D_{h_{in}}$, $z/D_{h_{in}}$)

Greek Symbols

Γ	Perimeter (m)
θ	Dimensionless temperature ($\frac{T-T_{in}}{\frac{q''D_h}{k_{bf}}}$)
γ	Convergence ratio (W_O/W_i)
μ	Viscosity (kg/m s)

ρ	Density (kg/m^3)
$\emptyset$	Volume fraction

Subscripts

ave	Average
app	Apparent
b	Bulk
bf	Base fluid
c	Cross-section
in	Inlet
eff	Effective
h	Hydraulic
nf	Nanofluid
p	Particle
s	Solid
w	Wall

Superscripts

+,*	Dimensionless values

Acknowledgements

The corresponding author is grateful for the support of the Iran National Science Foundation "INSF" (grant number 98026934).

References

[1] Modjinou, M., Ji, J., Yuan, W., Zhou, F., Holliday, S., Waqas, A. and Zhao, X., 2019. Performance comparison of encapsulated PCM PV/T, microchannel heat pipe PV/T and conventional PV/T systems. *Energy*, *166*, pp.1249-1266.

[2] Deng, D., Xie, Y., Chen, L., Pi, G. and Huang, Y., 2019. Experimental investigation on thermal and combustion performance of a combustor with microchannel cooling. *Energy*, *181*, pp.954-963.

[3] Osanloo, B., Mohammadi-Ahmar, A., Solati, A. and Baghani, M., 2016. Performance enhancement of the double-layered micro-channel heat sink by use of tapered channels. *Applied Thermal Engineering*, *102*, pp.1345-1354.

[4] Bejan, A., 2013. *Convection heat transfer*. John wiley & sons.

[5] Li, J., Peterson, G.P. and Cheng, P., 2004. Three-dimensional analysis of heat transfer in a micro-heat sink with single phase flow. *International Journal of Heat and Mass Transfer*, *47*(19-20), pp.4215-4231.

[6] Gamrat, G., Favre-Marinet, M. and Asendrych, D., 2005. Conduction and entrance effects on laminar liquid flow and heat transfer in rectangular microchannels. *International Journal of Heat and Mass Transfer*, *48*(14), pp.2943-2954.

[7] Akar, S., Rashidi, S., Esfahani, J.A. and Karimi, N., 2019. Targeting a channel coating by using magnetic field and magnetic nanofluids. *Journal of Thermal Analysis and Calorimetry*, *137*(2), pp.381-388.

[8] Akbarzadeh, M., Rashidi, S., Karimi, N. and Ellahi, R., 2018. Convection of heat and thermodynamic irreversibilities in two-phase, turbulent nanofluid flows in solar heaters by corrugated absorber plates. *Advanced Powder Technology*, *29*(9), pp.2243-2254.

[9] Rashidi, S., Karimi, N., Sunden, B., Mahian, O. and Harmand, S., 2020. Passive techniques to enhance heat transfer in various thermal systems. *Journal of Thermal Analysis and Calorimetry*, *140*(3), pp.875-878.

[10] Koo, J. and Kleinstreuer, C., 2005. Laminar nanofluid flow in microheat-sinks. *International journal of heat and mass transfer*, *48*(13), pp.2652-2661.

[11] Jang, S.P. and Choi, S.U., 2006. Cooling performance of a microchannel heat sink with nanofluids. *Applied Thermal Engineering*, *26*(17-18), pp.2457-2463.

[12] Wen, D. and Ding, Y., 2004. Experimental investigation into convective heat transfer of nanofluids at the entrance region under laminar flow conditions. *International journal of heat and mass transfer*, *47(24)*, pp.5181-5188.

[13] Fornalik-Wajs, E., Roszko, A. and Donizak, J., 2020. Nanofluid flow driven by thermal and magnetic forces–Experimental and numerical studies. *Energy*, *201*, p.117658.

[14] Hung, T.C., Sheu, T.S. and Yan, W.M., 2012. Optimal thermal design of microchannel heat sinks with different geometric configurations. *International communications in heat and mass transfer*, *39*(10), pp.1572-1577.

[15] He, Y., Men, Y., Zhao, Y., Lu, H. and Ding, Y., 2009. Numerical investigation into the convective heat transfer of TiO2 nanofluids flowing through a straight tube under the laminar flow conditions. *Applied Thermal Engineering*, *29*(10), pp.1965-1972.

[16] Mirzaei, M. and Dehghan, M., 2013. Investigation of flow and heat transfer of nanofluid in microchannel with variable property approach. *Heat and Mass Transfer*, *49*(12), pp.1803-1811.

[17] Chein, R. and Huang, G., 2005. Analysis of microchannel heat sink performance using nanofluids. *Applied thermal engineering*, *25*(17-18), pp.3104-3114.

[18] Peng, H., Guo, W. and Li, M., 2020. Thermal-hydraulic and thermodynamic performances of liquid metal based nanofluid in parabolic trough solar receiver tube. *Energy*, *192*, p.116564.

[19] Wang, Y., Li, Q. and Xuan, Y., 2019. Thermal and chemical reaction performance analyses of solar thermochemical volumetric receiver/reactor with nanofluid. *Energy*, *189*, p.116123.

[20] Huaxu, L., Fuqiang, W., Dong, L., Jie, Z. and Jianyu, T., 2019. Optical properties and transmittances of ZnO-containing nanofluids in spectral splitting photovoltaic/thermal systems. *International Journal of Heat and Mass Transfer*, *128*, pp.668-678.

[21] Huaxu, L., Fuqiang, W., Dong, Z., Ziming, C., Chuanxin, Z., Bo, L. and Huijin, X., 2020.

Experimental investigation of cost-effective ZnO nanofluid based spectral splitting CPV/T system. *Energy*, *194*, p.116913.

[22] Aminfar, H., Mohammadpourfard, M. and Kahnamouei, Y.N., 2011. A 3D numerical simulation of mixed convection of a magnetic nanofluid in the presence of non-uniform magnetic field in a vertical tube using two phase mixture model. *Journal of Magnetism and Magnetic Materials*, *323*(15), pp.1963-1972.

[23] Wrobel, W., Fornalik-Wajs, E. and Szmyd, J.S., 2010. Experimental and numerical analysis of thermo-magnetic convection in a vertical annular enclosure. *International Journal of Heat and Fluid Flow*, *31*(6), pp.1019-1031.

[24] Sawada, T., Tanahashi, T. and Ando, T., 1987. Two-dimensional flow of magnetic fluid between two parallel plates. *Journal of Magnetism and Magnetic Materials*, *65*(2-3), pp.327-329.

[25] Selimli, S., Recebli, Z. and Arcaklioglu, E., 2015. MHD numerical analyses of hydrodynamically developing laminar liquid lithium duct flow. *International Journal of Hydrogen Energy*, *40*(44), pp.15358-15364.

[26] Zhao, M. and Hu, J., 2012, December. Study on density of magnetic fluid in the strong magnetic field. In *2012 Second International Conference on Instrumentation, Measurement, Computer, Communication and Control* (pp. 396-398). IEEE.

[27] Hajialigol, N., Fattahi, A., Ahmadi, M.H., Qomi, M.E. and Kakoli, E., 2015. MHD mixed convection and entropy generation in a 3-D microchannel using Al2O3–water nanofluid. *Journal of the Taiwan Institute of Chemical Engineers*, *46*, pp.30-42.

[28] Aminfar, H., Mohammadpourfard, M. and Zonouzi, S.A., 2013. Numerical study of the ferrofluid flow and heat transfer through a rectangular duct in the presence of a non-uniform transverse magnetic field. *Journal of Magnetism and Magnetic materials*, *327*, pp.31-42.

[29] Ganguly, R., Sen, S. and Puri, I.K., 2004. Heat transfer augmentation using a magnetic fluid under the influence of a line dipole. *Journal of Magnetism and Magnetic Materials*, *271*(1), pp.63-73.

[30] Fadaei, F., Shahrokhi, M., Dehkordi, A.M. and Abbasi, Z., 2017. Heat transfer enhancement of Fe3O4 ferrofluids in the presence of magnetic field. *Journal of Magnetism and Magnetic Materials*, *429*, pp.314-323.

[31] Zeng, J., Deng, Y., Vedantam, P., Tzeng, T.R. and Xuan, X., 2013. Magnetic separation of particles and cells in ferrofluid flow through a straight microchannel using two offset magnets. *Journal of Magnetism and Magnetic Materials*, *346*, pp.118-123.

[32] Sheikholeslami, M., Bandpy, M.G., Ellahi, R. and Zeeshan, A., 2014. Simulation of MHD CuO–water nanofluid flow and convective heat transfer considering Lorentz forces. *Journal of Magnetism and Magnetic Materials*, *369*, pp.69-80.

[33] Zborowski, M., Sun, L., Moore, L.R., Williams, P.S. and Chalmers, J.J., 1999. Continuous cell separation using novel magnetic quadrupole flow sorter. *Journal of magnetism and magnetic materials*, *194*(1-3), pp.224-230.

[34] Hoyos, M., Moore, L., Williams, P.S. and Zborowski, M., 2011. The use of a linear Halbach array combined with a step-SPLITT channel for continuous sorting of magnetic species. *Journal of magnetism and magnetic materials*, *323*(10), pp.1384-1388.

[35] Dehghan, M., Daneshipour, M. and Valipour, M.S., 2018. Nanofluids and converging flow passages: A synergetic conjugate-heat-transfer enhancement of micro heat sinks. *International Communications in Heat and Mass Transfer*, *97*, pp.72-77.

[36] Dehghan, M., Vajedi, H., Daneshipour, M., Pourrajabian, A., Rahgozar, S. and Ilis, G.G., 2020. Pumping power and heat transfer rate of converging microchannel heat sinks: errors associated with the temperature dependency of nanofluids. *Journal of Thermal Analysis and Calorimetry*, *140*(3), pp.1267-1275.

[37] Dehghan, M., Daneshipour, M., Valipour, M.S., Rafee, R. and Saedodin, S., 2015. Enhancing heat transfer in microchannel heat sinks using converging flow passages. *Energy Conversion and Management*, *92*, pp.244-250.